

Effect of interfacial dislocations on ferroelectric phase stability and domain morphology in a thin film—a phase-field model

S. Y. Hu, Y. L. Li,^{a)} and L. Q. Chen

Department of Materials Science and Engineering, The Pennsylvania State University, University Park, Pennsylvania 16802

(Received 13 January 2003; accepted 15 May 2003)

A phase-field model was developed for predicting the domain structure evolution in a thin film with an arbitrary distribution of dislocations and subject to a substrate constraint. The effect of interfacial dislocations on the formation of tetragonal ferroelectric domains in a cubic paraelectric matrix was studied. It was found that the presence of interfacial dislocations locally modifies the ferroelectric transition temperature and leads to the preferential formation of ferroelectric domains around misfit dislocations. The types of tetragonal variants depend on the directions of the dislocation lines and their Burgers vectors. © 2003 American Institute of Physics. [DOI: 10.1063/1.1590416]

I. INTRODUCTION

The nature of the ferroelectric phase transition and the resulting domain structure evolution can be significantly affected by the presence of internal electrical and structural defects. A defect can locally modify the atomic bonding and thus the local transition temperature. It can also influence the phase transition through the field that it generates. In a phenomenological description using the Landau theory, the leading contribution of defects to the total free energy can be simply described by¹

$$f_d = \frac{\Delta A(\mathbf{x})}{2} \eta^2(\mathbf{x}) - h_d(\mathbf{x}) \eta(\mathbf{x}), \quad (1)$$

where $\mathbf{x} = (x_1, x_2, x_3)$ is the spatial location, $\eta(\mathbf{x})$ is the order parameter describing the phase transition, $\Delta A(\mathbf{x})$ is the change in the coefficient of the second-order term in the Landau expansion due to the presence of defects, and $h_d(\mathbf{x})$ is the local field produced by the defects, which may produce nonzero local values for the order parameter even above the Curie temperature.

In this work, we consider a special type of structural defect, namely, dislocations, which generate inhomogeneous elastic fields. Our focus is on the effect of interfacial dislocations on the formation of ferroelectric domains in a thin film. Interfacial dislocations are generated to release the strain energy arising from a lattice mismatch between a film and a substrate.² The effect of interfacial dislocations on ferroelectric domain formation in thin films has been discussed previously using the reduced average substrate constraint due to the formation of misfit dislocations.^{3–7} In this study, we consider both the average macro effect of a substrate and the local effect on the ferroelectric phase transition and the accompanying domain formation. For this purpose, we use the phase-field approach. Phase-field approach has previously been applied by Leonard and Desai to modeling a similar problem, phase separation in a binary thin film with dislocations.⁸ However, since they employed analytical elas-

tic solutions to incorporate dislocations, it is difficult to apply their method to cases with an arbitrary distribution of dislocations. In this work, we focus on the ferroelectric phase transformations and domain structure evolution in a thin film with an arbitrary distribution of dislocations.

II. PHASE-FIELD MODEL

A ferroelectric transition from cubic to tetragonal is considered. The bulk thermodynamics in a stress-free state is described by a Landau expansion using the unpolarized and unstressed crystal as the reference,

$$\begin{aligned} f_{\text{Lan}} = & \alpha_1 (P_1^2 + P_2^2 + P_3^2) + \alpha_{11} (P_1^4 + P_2^4 + P_3^4) \\ & + \alpha_{12} (P_1^2 P_2^2 + P_2^2 P_3^2 + P_3^2 P_1^2) + \alpha_{111} (P_1^6 + P_2^6 + P_3^6) \\ & + \alpha_{112} [P_1^2 (P_2^4 + P_3^4) + P_2^2 (P_1^4 + P_3^4) \\ & + P_3^2 (P_1^4 + P_2^4)] + \alpha_{123} P_1^2 P_2^2 P_3^2, \end{aligned} \quad (2)$$

where $\mathbf{P} = (P_1, P_2, P_3)$ is the polarization vector, and α_1 , α_{11} , α_{12} , α_{111} , α_{112} , and α_{123} are phenomenological coefficients which determine the nature of the transition, the transition temperature, and the dielectric susceptibility as a function of temperature. It should be emphasized that the set of coefficients in Eq. (2) is measured under the stress-free boundary condition.

Under the stress-free condition, the ferroelectric phase transition is accompanied by a spontaneous strain (called the eigenstrain in micromechanics)

$$\epsilon_{ij}^{0P} = Q_{ijkl} P_k P_l, \quad (3)$$

where Q_{ijkl} is the electrostrictive coefficient tensor, and the superscript P means the eigenstrain arising from the polarization.

In the phase-field model, the domain structure is described by a spatially inhomogeneous polarization distribution. Therefore, the eigenstrain is also inhomogeneous in the domain structure, resulting in long-range anisotropic elastic interactions among ferroelectric domains. Similarly, any arbitrary spatial distribution of dislocations can be described

^{a)}Corresponding author. Electronic mail: yill@psu.edu

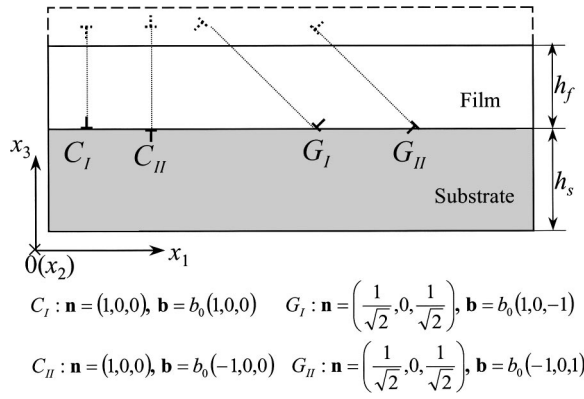


FIG. 1. Schematic illustrations of simulation model and dislocations.

by a space-dependent eigenstrain distribution. For example, a dislocation loop on slip plane s with a Burgers vector $\mathbf{b} = (b_1, b_2, b_3)$ can be expressed through the stress-free eigenstrain^{9,10}

$$\epsilon_{ij}^{0D} = \frac{1}{2d_0} [(b_i n_j + b_j n_i)] \delta(\mathbf{x} - \mathbf{x}^D), \quad (4)$$

where $\mathbf{n} = (n_1, n_2, n_3)$ is the unit vector normal to the slip plane, d_0 is the interplanar distance of the slip plane, $\delta(\mathbf{x} - \mathbf{x}^D)$ is the Dirac function, and \mathbf{x}^D is a point inside the dislocation loop. Therefore, for a spatial distribution of many dislocation loops, the associated eigenstrain can be obtained by considering the total eigenstrains due to all individual dislocation loops. We consider film-substrate interfacial dislocations with dislocation lines parallel to x_2 axis (see Fig. 1). In order to describe the interfacial dislocations using dislocation loops, image dislocations are introduced, as shown in Fig. 1 by the dotted dislocation symbols.

With the total eigenstrain for a domain structure with dislocations $\epsilon_{ij}^0 = \epsilon_{ij}^{0P} + \epsilon_{ij}^{0D}$, the elastic strains and stresses can be obtained by solving the mechanical equilibrium equation, through a combination of Stroh's algorithm and the mesoscopic elasticity theory of Khachaturyan.¹¹⁻¹⁵ The mechanical equilibrium equation is given by

$$\frac{\partial \sigma_{ij}}{\partial x_j} = \frac{\partial (c_{ijkl} e_{kl})}{\partial x_j} = 0, \quad (5)$$

where e_{ij} is the elastic strain component, which can be obtained by subtracting the stress-free eigenstrain ϵ_{ij}^0 from the total strain ϵ_{ij} , i.e., $e_{ij} = \epsilon_{ij} - \epsilon_{ij}^0$, and c_{ijkl} is the elastic stiffness tensor.

To validate the elastic solution, we compared the stress field obtained from the present approach and that from the analytical solution¹⁶ for the case of a climb or glide dislocation in a half plane, assuming isotropic elasticity. It was found that our numerical solution agrees very well with the analytical solution (see Fig. 2).

The elastic energy density of a domain structure is given by

$$f_{\text{ela}} = \frac{1}{2} c_{ijkl} e_{ij} e_{kl}. \quad (6)$$

Expanding Eq. (6), we have

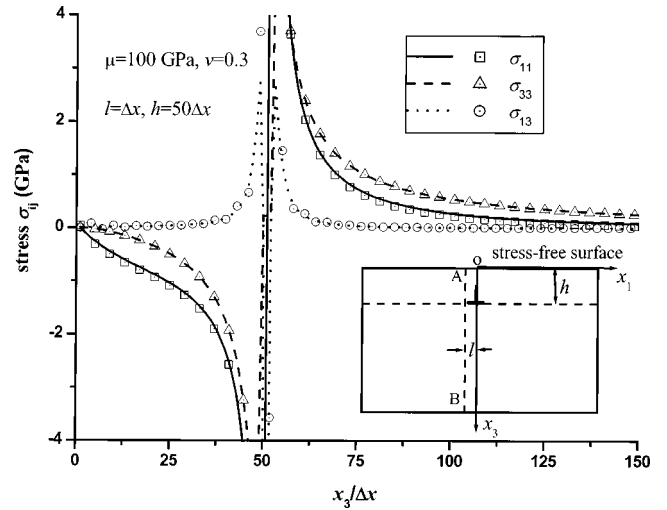


FIG. 2. Comparison of stresses from analytical solution (lines) and from our numerical calculation (scatter symbols) of an edge dislocation in an elastically isotropic half space with shear modulus μ and Poisson's ratio ν . The plotted stresses are along the dashed line of AB.

$$\begin{aligned} f_{\text{ela}} &= \frac{1}{2} c_{ijkl} e_{ij} e_{kl} = \frac{1}{2} c_{ijkl} (\epsilon_{ij} - \epsilon_{ij}^{0D} - \epsilon_{ij}^{0P}) (\epsilon_{kl} - \epsilon_{kl}^{0D} - \epsilon_{kl}^{0P}) \\ &= \frac{1}{2} c_{ijkl} (\epsilon_{ij} - \epsilon_{ij}^{0D} - Q_{ijmn} P_m P_n) \\ &\quad \times (\epsilon_{kl} - \epsilon_{kl}^{0D} - Q_{klmn} P_m P_n) \\ &= \frac{1}{2} c_{ijkl} Q_{ijmn} Q_{klst} P_m P_n P_s P_t \\ &\quad - c_{ijkl} (\epsilon_{ij} - \epsilon_{ij}^{0D}) Q_{klmn} P_m P_n \\ &\quad + \frac{1}{2} c_{ijkl} (\epsilon_{ij} - \epsilon_{ij}^{0D}) (\epsilon_{kl} - \epsilon_{kl}^{0D}). \end{aligned} \quad (7)$$

It is seen that the introduction of elastic energy alters the coefficients of the quadratic and fourth-order terms in the bulk Landau free energy polynomial in Eq. (2). Since the eigenstrain describing the misfit dislocations is spatially inhomogeneous, it is easy to see that the presence of dislocations modifies the local properties inside a ferroelectric domain in which the polarization is otherwise homogeneous.

For simplicity, we consider only the effect of elastic fields and ignore the explicit change in local atomic bonding due to the presence of misfit dislocations. We assume that the interfacial dislocations are generated during a film deposition, and no additional dislocation forms during cooling. We also assume that the dislocations do not move during domain evolution. The effect of mobile dislocations will be considered in a future publication.

The temporal evolution of a ferroelectric domain structure is described by the time-dependent Ginzburg-Landau equation

$$\frac{\partial P_i(\mathbf{x}, t)}{\partial t} = -L \frac{\delta F}{\delta P_i(\mathbf{x}, t)} \quad (i = 1, 2, 3), \quad (8)$$

where L is related to domain-wall mobility, F is the total free energy of the film, and t is time. The total free energy in-

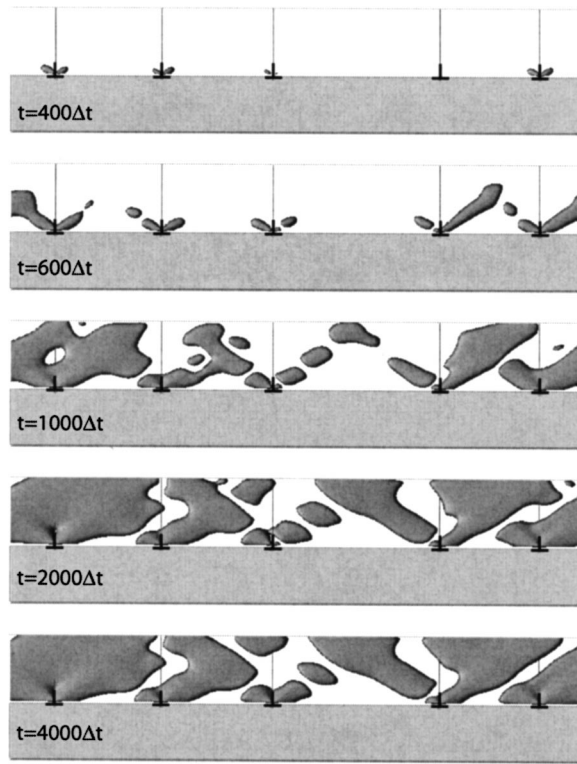


FIG. 3. Temporal morphologies of ferroelectric domains (c domains) at $T = 485^\circ\text{C}$ in PbTiO_3 film in the presence of C_1 -type interfacial dislocations.

cludes the bulk free energy, domain wall energy, elastic energy, electric energy, and surface and interface contributions. The domain-wall energy is introduced through gradients of the polarization field.^{15,17,18} Since this work emphasizes the effect of film/substrate interfacial dislocations, the interfacial contributions and the electric energy are ignored. The effect of electric energy was discussed in one of our previous papers.¹⁸

III. RESULTS AND DISCUSSION

Numerical simulations of ferroelectric domain formation were carried out by solving Eq. (8) using the semi-implicit Fourier-spectral method.¹⁹ A lead titanate (PbTiO_3) thin film is considered.²⁰ The coefficients of the Landau free energy expansion as well as the electrostrictive and elastic constants are listed in Ref. 21, adapted from Refs. 22 and 23. With this set of coefficients, the transition is first order in the bulk under stress-free conditions. However, it becomes second order under clamped boundary conditions. Therefore, the paraelectric to ferroelectric transition is continuous or spinodal under a substrate constraint in the sense that nucleation of ferroelectric domains in a paraelectric matrix is barrierless. A computational cell size of $512\Delta x \times 1\Delta x \times 128\Delta x$ was employed with $\Delta x = d_0$ being the grid size for the spatial discretization. Periodic boundary conditions are applied along the x_1 and x_2 axes lying along the film plane. Since only one grid point is used in one of the dimensions, the simulation is essentially two dimensional. However, since our main interest is in studying the initial nucleation of domains around misfit dislocations, this quasi-two-dimensional

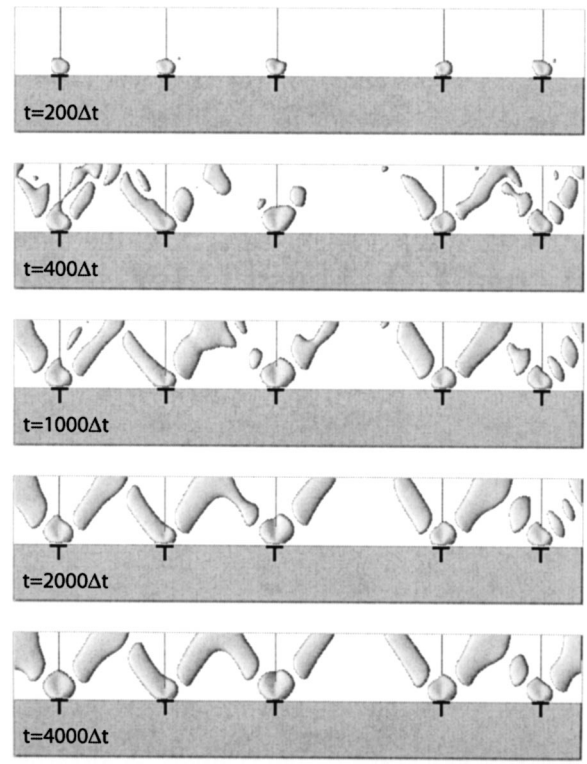


FIG. 4. Temporal morphologies of ferroelectric domains (a domains) at $T = 485^\circ\text{C}$ in PbTiO_3 film in the presence of C_{II} -type interfacial dislocations.

system is sufficient, although the equilibrium volume fractions of each domain variant may not be accurate due to this two-dimensional nature. The film thickness was taken as $h_f = 60\Delta x$, and the heterogeneous elastic deformation in the substrate is limited to a distance of $h_s = 54\Delta x$ from the film/substrate interface. The parameters defining the dislocation eigenstrain are chosen as $b_0/d_0 = 1/3$. The dimensionless time increment (in units of $1/L$) was taken as $\Delta t = 0.06$.

The transition temperature for PbTiO_3 from the paraelectric cubic phase to the ferroelectric tetragonal phase was $T_c = 479^\circ\text{C}$ under clamped boundary conditions with zero strain. Therefore, in the absence of any local strain field, the paraelectric cubic phase is stable at a temperature higher than T_c . In the presence of dislocations, however, the inhomogeneous strain field of dislocations leads to the variation of transition temperatures in space, and it is possible for the ferroelectric phase to appear at a temperature higher than the bulk T_c . The local transition temperature can be determined from the modified coefficient of P_m^2 ,

$$\alpha'_m = \alpha_1 + \Delta\alpha_m, \quad (9)$$

$$\Delta\alpha_m = -c_{ijkl}(\epsilon_{kl} - \epsilon_{kl}^{0D})Q_{ijmm}, \quad (10)$$

where no summation is taken for the repeated m . If $\alpha'_m < 0$, the paraelectric phase is unstable with respect to its transition to a ferroelectric phase.

To study the domain formation, we started the simulation from a high-temperature paraelectric state. The initial state was generated by assigning a zero value at each grid point for each component of the polarization field plus a small random noise of uniform distribution. The average substrate

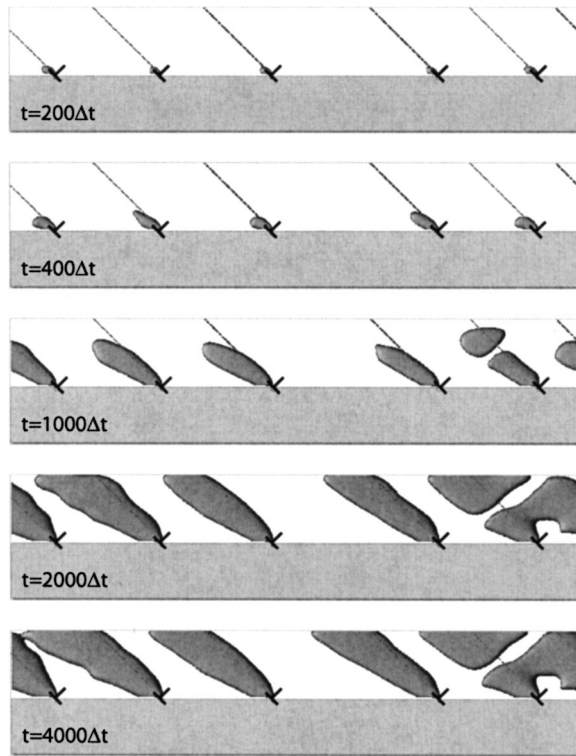


FIG. 5. Temporal morphologies of ferroelectric domains (*c* domains) at $T = 485^\circ\text{C}$ in PbTiO_3 film in the presence of G_I -type interfacial dislocations.

constraint was fixed to be zero, implying the lattice parameter of the film along the film plane is constrained to the value corresponding to the stress-free paraelectric state during a ferroelectric phase transition. Our simulation showed

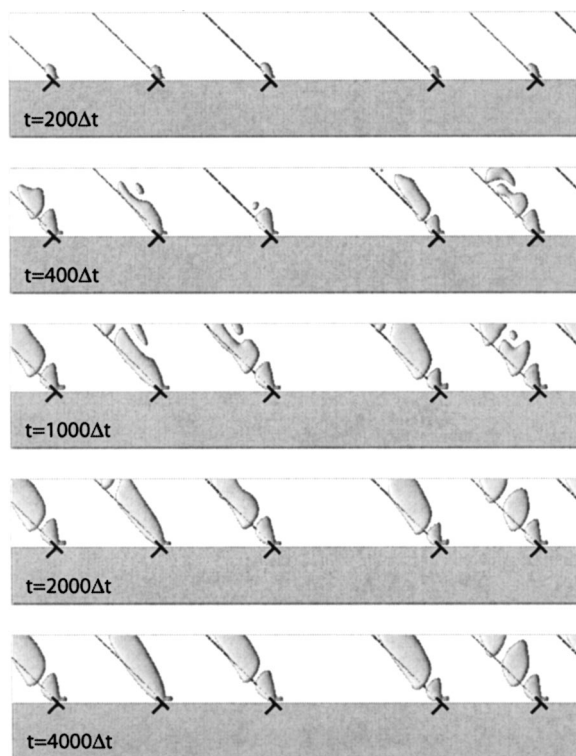


FIG. 6. Temporal morphologies of ferroelectric domains (*a* domains) at $T = 485^\circ\text{C}$ in PbTiO_3 film in the presence of G_{II} -type interfacial dislocations.

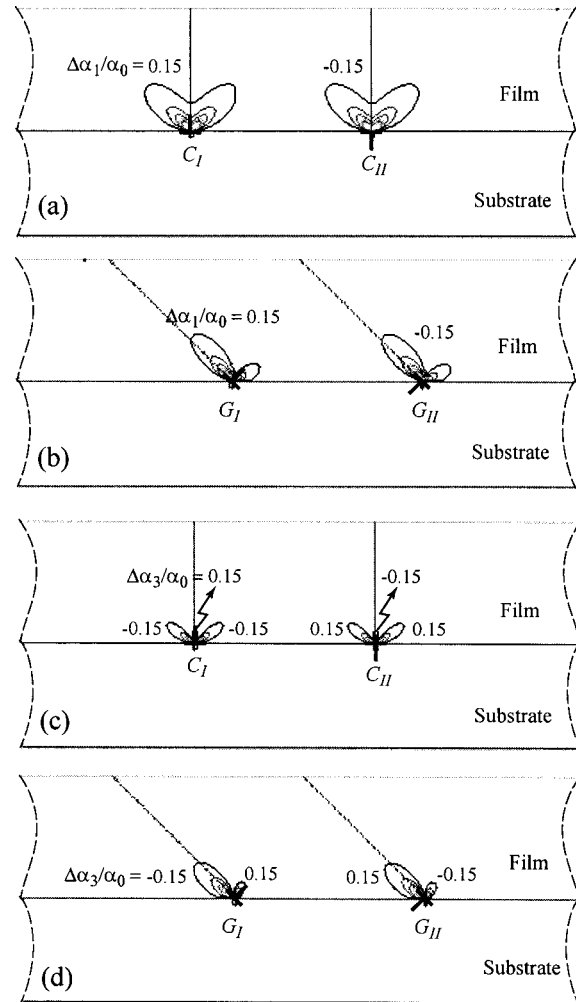
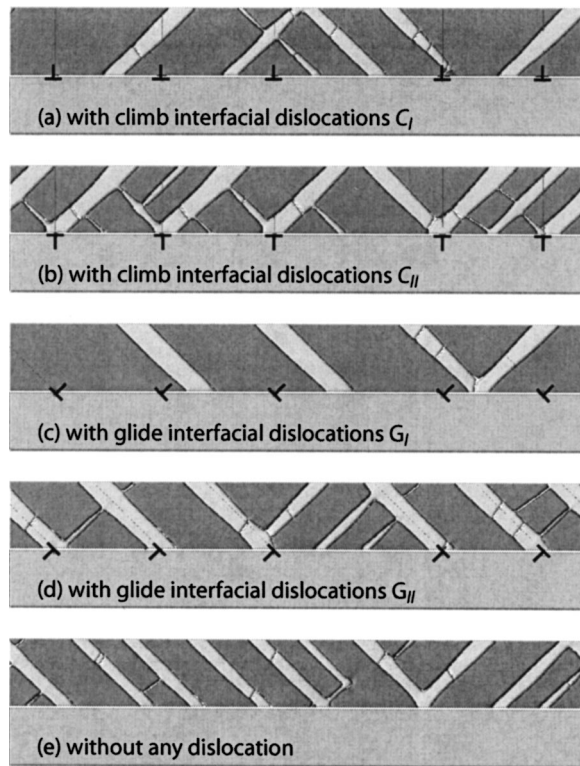


FIG. 7. Spatial distributions of $\Delta\alpha_1$ and $\Delta\alpha_3$ in Eqs. (9) and (10) around the given interfacial dislocations. The plotted contours are based on the value of $\Delta\alpha_m/\alpha_0$ ($\alpha_0 = |\alpha_1|_{T=25^\circ\text{C}}$). The outermost contour corresponds to the value of $|\Delta\alpha_m/\alpha_0| = 0.15$ while the inner contours are drawn with increasing values of $|\Delta\alpha_m/\alpha_0|$ at intervals of 0.1.

that the ferroelectric phase does not nucleate from the paraelectric parent phase in the absence of misfit dislocations at 485°C . When interfacial dislocations were introduced, ferroelectric phases appeared around the dislocations at the same temperature.

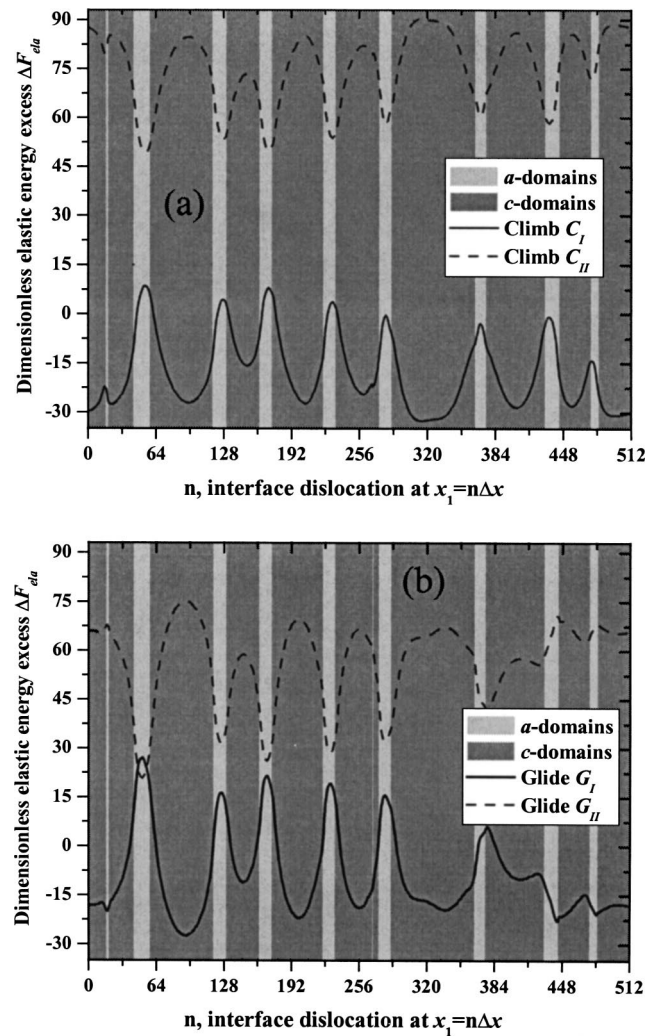
The spatial distribution of the ferroelectric tetragonal phase at $T = 485^\circ\text{C}$ is shown in Figs. 3–6 for the four types of dislocations C_I , C_{II} , G_I , and G_{II} (see Fig. 1 for the definition of the types of dislocations). In the figures, the substrate and the ferroelectric *a* domains of $(\pm P_1, 0, 0)$ and *c* domains of $(0, 0, \pm P_3)$ are shown in gray, light gray, and dark gray, respectively. The domain structures were plotted using the contours of $|P_i|/P_s = 0.5$ where P_s is the stress-free spontaneous polarization at the corresponding temperature. The bright regions in the film represent the parent cubic phase. The black straight lines label the dislocation slip planes and dislocation locations. It is shown that both the climb C_I and glide G_I types of dislocation favor the formation of *c* domains, whereas *a* domains preferentially nucleate around climb C_{II} and glide G_{II} dislocations. For different types of dislocation, both the location of the initial ferroelec-

FIG. 8. Domain structure morphologies at $T=25^\circ\text{C}$.

tric domains and the rate of domain growth are different. For example, ferroelectric domains nucleate at both sides of a climb dislocation but only at one side of a glide dislocation. For each case there is only one kind of domain, either a or c domains, i.e., two types of domain cannot form simultaneously around the same type of dislocation. This observation can be easily explained by the spatial variation of $\Delta\alpha_m$ in Eqs. (9) and (10). Figure 7 shows the contours of $\Delta\alpha_1$ and $\Delta\alpha_3$ based on the value of $\Delta\alpha_m/\alpha_0$ ($\alpha_0=|\alpha_1|_{T=25^\circ\text{C}}$). The a and c domains are favored to form in the regions where $\Delta\alpha_1$ and $\Delta\alpha_3$ have negative values, respectively. It is seen that both the C_I and G_I types of dislocation favor c domains. The c domains form at both sides of a C_I dislocation but only at the left-hand side of a G_I dislocation, which is clearly shown by the variation of $\Delta\alpha_3/\alpha_0$. Similarly, C_{II} and G_{II} types of dislocation favor a domains. It was observed that the domain structures show little change for $t \geq 4000\Delta t$ at the given temperature.

After 4000 time steps of annealing at $T=485^\circ\text{C}$, we decrease the temperature in steps of 10°C and hold the system at each temperature for 200 time steps. Figure 8 presents the domain morphologies at room temperature, $T=25^\circ\text{C}$. For comparison, a domain structure without the presence of dislocations is also shown in Fig. 8. It is interesting to observe that the dislocations are always located inside the ferroelectric domains, either c or a domains, depending on the type of dislocation. Moreover, the domains having dislocation inside have larger sizes compared with the domains without dislocations. Dislocations inside domains have also been observed experimentally.^{20,24}

In the work of Dai *et al.*²⁴ it was pointed out that a

FIG. 9. Elastic energy excess ΔF_{ela} versus the position of the dislocation due to the insertion of an interface dislocation. The light-gray and dark-gray stripes just indicate the a and c domains along the film/substrate interface, the same as those shown in Fig. 8(e).

domain boundary is likely to be pinned by dislocations. However, our simulations revealed that dislocations prefer to be located inside the ferroelectric domains. In order to investigate the energetically favorable locations for dislocations, we made a numerical calculation, i.e., we inserted a dislocation in a ferroelectric domain structure and examined its interaction with the domain structure. Figure 8(e) is the domain structure without dislocations. After inserting a dislocation, we calculated the elastic energy excess ΔF_{ela} due to the insertion of the dislocation. Plots of ΔF_{ela} versus the position of dislocation are presented in Fig. 9 for the four types of dislocation considered in this work. The light-gray and dark-gray stripes indicate the a and c domains along the film/substrate interface. Negative values of ΔF_{ela} mean that the elastic energy is lower with the presence of a dislocation, i.e., the existence of the dislocation is energetically favored. It is found that ΔF_{ela} reaches a minimum (negative values) mostly when the C_I or G_I type of dislocation is inserted in the middle region of a ferroelectric c domain. That is, for the given domain structure in Fig. 8(e), an inserted dislocation of the C_I or G_I type is energetically favored to locate inside the

c domains. The C_{II} or G_{II} types of dislocation always increase the total free energy of the system. However, if a dislocation of either the C_{II} or G_{II} type is present at the interface, it prefers to be in the middle of an a domain where ΔF_{ela} is minimum. The energetic analysis agrees with our simulation shown in Figs. 8(c)–8(d). It is interesting to note that ΔF_{ela} also has a local minimum at a domain boundary that is parallel to the normal of the dislocation slide plane [see the left sides of Figs. 8(e) and 9(b)], implying that a dislocation of the G_I type could be locally pinned at a domain boundary due to the elastic interactions. It should be borne in mind that the dislocation core energy is ignored in all of our calculations.

IV. CONCLUSION

A phase-field model is developed for predicting domain structure evolution in a ferroelectric thin film with arbitrary spatial distribution of dislocations and subject to a substrate constraint. The micromechanical concept of “eigenstrain” is employed to describe the discontinuous displacement within dislocation loops on slip planes. An elastic solution is obtained for a thin film with an eigenstrain distribution associated with a distribution of dislocations and domains. The effect of interfacial dislocations on ferroelectric domain nucleation and growth was simulated. Based on the elastic interactions, the interfacial dislocations are energetically favored to locate inside a ferroelectric domain instead of at domain walls.

ACKNOWLEDGMENTS

Financial support by the National Science Foundation under Grants No. DMR-0103354 and No. DMR-0122638 is gratefully acknowledged.

¹A. P. Levanyuk and A. S. Sigov, *Defects and Structural Phase Transitions*, Vol. 6 (Gordon and Breach, New York, 1988).

- ²J. W. Matthews and A. E. Blakeslee, *J. Cryst. Growth* **27**, 118 (1974).
³J. S. Speck and W. Pompe, *J. Appl. Phys.* **76**, 466 (1994).
⁴J. S. Speck, A. C. Daykin, A. Seifert, A. E. Romanov, and W. Pompe, *J. Appl. Phys.* **78**, 1696 (1995).
⁵A. E. Romanov, W. Pompe, and J. S. Speck, *J. Appl. Phys.* **79**, 4037 (1996).
⁶S. P. Alpay, A. S. Prakash, S. Aggarwal, P. Shuk, M. Greenblatt, R. Ramesh, and A. L. Roytburd, *Scr. Mater.* **39**, 1435 (1998).
⁷S. P. Alpay and A. L. Roytburd, *J. Appl. Phys.* **83**, 4714 (1998).
⁸F. Leonard and R. C. Desai, *Phys. Rev. B* **58**, 8277 (1998).
⁹S. Y. Hu and L. Q. Chen, *Acta Mater.* **49**, 463 (2001).
¹⁰Y. U. Wang, Y. M. Jin, A. M. Cuitino, and A. G. Khachaturyan, *Appl. Phys. Lett.* **78**, 2324 (2001).
¹¹A. G. Khachaturyan and G. A. Shatalov, *Sov. Phys. JETP* **29**, 557 (1969).
¹²A. G. Khachaturyan, *Theory of Structural Transformation in Solids* (Wiley, New York, 1983).
¹³A. N. Stroh, *J. Math. Phys.* **41**, 77 (1962).
¹⁴T. C. T. Ting, *Anisotropic Elasticity, Theory and Applications* (Oxford University Press, New York, 1996).
¹⁵Y. L. Li, S. Y. Hu, Z. K. Liu, and L. Q. Chen, *Acta Mater.* **50**, 395 (2002).
¹⁶V. L. Indenbom and J. Lothe, *Elastic Strain Fields and Dislocation Mobility*, Vol. 31, 1st ed. (Elsevier, North-Holland, 1992).
¹⁷Y. L. Li, S. Y. Hu, Z. K. Liu, and L. Q. Chen, *Appl. Phys. Lett.* **78**, 3878 (2001).
¹⁸Y. L. Li, S. Y. Hu, Z. K. Liu, and L. Q. Chen, *Appl. Phys. Lett.* **81**, 427 (2002).
¹⁹L. Q. Chen and J. Shen, *Comput. Phys. Commun.* **108**, 147 (1998).
²⁰S. Stemmer, S. K. Streiffner, F. Ernst, and M. Ruhle, *Phys. Status Solidi A* **147**, 135 (1995).
²¹PbTiO₃ material constants: $\alpha_1 = 3.8(T - 479) \times 10^5 \text{ C}^{-2} \text{ m}^2 \text{ N}$, $\alpha_{11} = -7.3 \times 10^7 \text{ C}^{-4} \text{ m}^6 \text{ N}$, $\alpha_{12} = 7.5 \times 10^8 \text{ C}^{-4} \text{ m}^6 \text{ N}$, $\alpha_{111} = 2.6 \times 10^8 \text{ C}^{-6} \text{ m}^{10} \text{ N}$, $\alpha_{112} = 6.1 \times 10^8 \text{ C}^{-6} \text{ m}^{10} \text{ N}$, $\alpha_{123} = -3.7 \times 10^9 \text{ C}^{-6} \text{ m}^{10} \text{ N}$, $Q_{11} = 0.089 \text{ C}^{-2} \text{ m}^4$, $Q_{12} = -0.026 \text{ C}^{-2} \text{ m}^4$, $Q_{44} = 0.03375 \text{ C}^{-2} \text{ m}^4$, $c_{11} = 1.746 \times 10^{11} \text{ N m}^{-2}$, $c_{12} = 7.937 \times 10^{10} \text{ N m}^{-2}$, $c_{44} = 1.111 \times 10^{11} \text{ N m}^{-2}$, where T is temperature in °C.
²²M. J. Haun, E. Furman, S. J. Jang, H. A. McKinstry, and L. E. Cross, *J. Appl. Phys.* **62**, 3331 (1987).
²³N. A. Pertsev, A. G. Zembilgotov, and A. K. Tagantsev, *Phys. Rev. Lett.* **80**, 1988 (1998).
²⁴Z. R. Dai, Z. L. Wang, X. F. Duan, and J. M. Zhang, *Appl. Phys. Lett.* **68**, 3093 (1996).